ACS Sustainable Chemistry & Engineering

pubs.acs.org/journal/ascecg

Research Article

NH_3 and HNO_x Formation and Loss in Nitrogen Fixation from Air with Water Vapor by Nonequilibrium Plasma

Elise Vervloessem,* Mikhail Gromov, Nathalie De Geyter, Annemie Bogaerts, Yury Gorbanev,‖ and Anton Nikiforov‖

Cite This: *ACS Sustainable Chem. Eng.* 2023, 11, 4289−4298

Read Online

ACCESS | Metrics & More | Article Recommendations | Supporting Information

ABSTRACT: The current global energy crisis indicated that increasing our insight into nonfossil fuel nitrogen fixation pathways for synthetic fertilizer production is more crucial than ever. Nonequilibrium plasma is a good candidate because it can use N_2 or air as a N source and water directly as a H source, instead of H_2 or fossil fuel (CH_4). In this work, we investigate NH_3 gas phase formation pathways from humid N_2 and especially humid air up to 2.4 mol % H_2O (100% relative humidity at 20 °C) by optical emission spectroscopy and Fourier-transform infrared spectroscopy. We demonstrate that the nitrogen fixation capacity is increased when water vapor is added, as this enables HNO_2 and NH_3 production in both N_2 and air. However, we identified a significant loss mechanism for NH_3 and HNO_2 that occurs in systems where these species are synthesized simultaneously; i.e., downstream from the plasma, HNO_2 reacts with NH_3 to form NH_4NO_2, which rapidly decomposes into N_2 and H_2O. We also discuss approaches to prevent this loss mechanism, as it reduces the effective nitrogen fixation when not properly addressed and therefore should be considered in future works aimed at optimizing plasma-based N_2 fixation. In-line removal of HNO_2 or direct solvation in liquid are two proposed strategies to suppress this loss mechanism. Indeed, using liquid H_2O is beneficial for accumulation of the N_2 fixation products. Finally, in humid air, we also produce NH_4NO_3, from the reaction of HNO_3 with NH_3, which is of direct interest for fertilizer application.

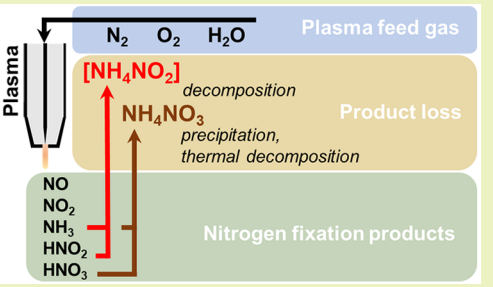

KEYWORDS: *Nitrogen fixation, Ammonia, Ammonium nitrite, Nonequilibrium plasma, Water vapor, Optical emission spectroscopy*

INTRODUCTION

Since the invention of synthetic fertilizers, food production increased drastically and enabled mass population expansion.[1] The most important industrial process in the field of nitrogen fixation (NF) (for, among others, synthetic fertilizer production) is the Haber-Bosh (HB) process: a thermo-catalytic conversion of N_2 and H_2 into ammonia.[2] While supporting 50% of the world's population,[3] the HB process depends on fossil fuels for energy and, for the majority of HB chemical plants, it is the hydrogen source[4,5] as well. The HB process has been extensively optimized during its 100-year existence, and there is currently no viable alternative or complementary process bringing the same support.[6] Because of the vital role synthetic fertilizers play and their accompanying high burden on the environment, it is of pivotal importance to research alternative ways for NF to ensure continuous improvement of synthetic fertilizer production. Although these alternative ways cannot fully substitute the HB process, they can present an appealing auxiliary technology of NF, especially in remote areas with abundant renewable electricity.[7] Moreover, because of the harsh conditions (high temperature and extreme pressure) required for its operation, the HB process is only economically feasible on large scales,[8] resulting in massive centralized production and subsequent costly distribution of the produced NH_3. Plasma-based NF is therefore an interesting method to consider as an alternative, because it is electricity-based and can use abundant feedstock like air, nitrogen, and water.[9,10] The process is decentralized, can operate on a scale which would fit the very local demand, and is operated at atmospheric pressure, resulting in an overall environmentally and economically friendly local small-scale production, which also eliminates transportation costs.

Plasma is an ionized gas, composed of electrons, photons, atoms, radicals, ions, and excited species. A variety of plasma sources and feed gases ($N_2/O_2/H_2/H_2O$ combinations) have been reported for plasma-based NF into NO_x[11−15] and NH_3 (in plasma-catalytic[16,17] and plasma-liquid[18] systems). A schematic overview is presented in Figure S1. Most of the reported plasma-based NH_3 production methods rely on H_2, often in the presence of a catalyst.[16,17] Although H_2 can be produced from water via electrolysis, a direct usage of water as

Received: January 11, 2023
Revised: February 15, 2023
Published: March 1, 2023

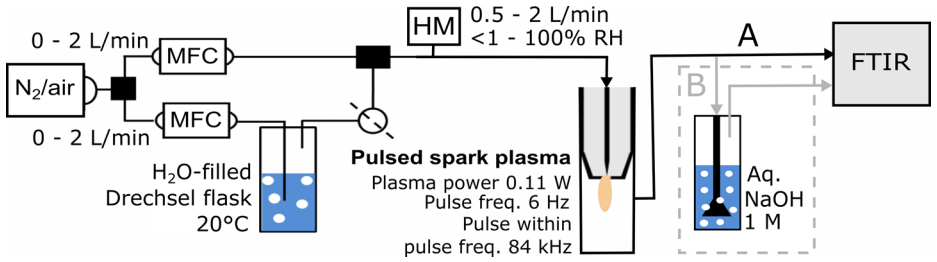

Figure 1. Experimental setup used in this work. Line A shows the setup where the effluent goes straight to the FTIR. Line B shows the setup where the effluent first passes a base washer, indicated by a dashed gray line. The latter is only used when specified in the text.

a hydrogen source is of interest for NH_3 production.[10,19] Therefore, studies of NH_3 formation and accumulation in plasma-treated water (PTW),[20−24] sometimes coupled to another technology, a UV source, an ozonator,[25−27] and/or an electrochemical cell,[28−30] have been gaining increased interest from both the scientific community and industry. Most of the advances in plasma-based nitrogen fixation are summarized in recent reviews.[10,31] We have previously shown that H_2O can also be used for the production of NH_3 from mixtures of N_2 and water vapor and, even more interestingly, from air (N_2 and O_2) and water vapor (i.e., humid air), with accumulation of the produced NH_3 in liquid water.[32] However, plasma-based studies that have looked at N_2/H_2O vapor and air/H_2O vapor (i.e., without liquid water) are very scarce.[32,33] Hence, more insight into the gas phase formation of NH_3 with water vapor is needed, not least to understand how NH_3 production can be achieved in both N_2 and air plasma using H_2O as a hydrogen source. In air/H_2O and N_2/H_2O mixtures, the formation of HNO_x is also of interest. The majority of fertilizers are ammonium salts produced from NH_3 and its oxidation product HNO_3, which is commercially synthesized through the Ostwald process using HB-made NH_3 as feedstock.[10] The direct synthesis of HNO_x alongside NH_3 could therefore result in a more streamlined production process.[34]

This work studies the selectivity of plasma-based NF in air and N_2 discharges at a relative humidity up to 100% at 20 °C (room temperature), i.e., up to 2.4 mol % H_2O. For this, we employed a pulsed plasma jet, which we previously used to study the underlying mechanisms responsible for the record-low energy consumption (EC) value in the case of NO_x generation from dry air,[35] ultimately yielding a very low overall EC for NH_3 production via plasma-formed NO_x further catalytically reduced into NH_3.[36] More importantly, we also used this plasma jet[32] to demonstrate that the gaseous H_2O present in the plasma feed gas (and not the liquid H_2O) plays the major role in NF, which was later also observed by Toth et al.[37] Moreover, we showed that both dissolved NH_4^+ and NO_x^- were formed when H_2O vapor was added to the plasma feed gas (N_2 or air). In the present work, we elaborate on this topic, investigating the fundamentals behind the one-step NF process from gaseous N_2/air and H_2O via gas phase diagnostics: Fourier-transform infrared spectroscopy (FTIR) and optical emission spectroscopy (OES) to elucidate the formation mechanisms of the H_2O-based NH_3.

EXPERIMENTAL SECTION

Plasma Setup. A plasma jet operating in a pulsed spark mode was used, as shown in Figure S2. The peak temperature in one pulse is 1750 ± 150 K; however, the time-averaged temperature is ca. 315 K. Detailed characterization of this device can be found in our previous works.[32,35] Based on the V/I waveforms and discharge imaging, the operational mode of the discharge in both low and high humidity was a low current spark, which is generated in between the pin electrode and the nozzle.[35] The typical duration of the spark is in the range of 700 ns. Due to the nature of the discharge, its characteristics did not change strongly with different humidity levels, as shown elsewhere.[32] The plasma jet was operating either in synthetic air (N_2 + O_2) or pure N_2 (both ≥99.999%, Air Liquide). The gas flow rate was regulated using two mass flow controllers (MFCs; EL-Flow, Bronkhorst). Partial saturation of the supplied feed gas with H_2O vapor was achieved by splitting the main gas flow and passing its fraction through a water-filled bubbler.[38,39] The resulting gaseous H_2O concentration in the flow was monitored with a humidity meter (Testo 445). The feed gas flow rate was 0.5 or 2 Ls/min (standard liters per minute; henceforth referred to as L/min for simplicity). All tubing in the setup was Swagelok PTFE (diameter 1/4 in.). The concentration of H_2O vapor was varied and will be shown in both molar percentage (<0.1 to 2.4 mol %) and relative humidity at 20 °C (<1 to 100%). We explicitly note that, even with no added H_2O vapor, the feed gas contained residual humidity, hence the absence of the zero value humidity. The effluent of the plasma jet was contained within a quartz reservoir (ca. 30 mL volume), the exhaust of which was connected to the FTIR spectrometer, as shown in Figure 1 (length ca. 50 cm).

Downstream Gas Phase Analysis. N-containing stable gaseous products were measured employing FTIR (Matrix-MG2, Bruker, 5 m optical path, using an average of 50 scans; all gas from the setup plasma was directed to the FTIR). Quantitative measurements of NO, NO_2, and N_2O were performed using Bruker's database and Beer's law based on the absorption cross sections from the HITRAN database.[40] The deviation between methods was found to be <3%. The concentrations of gaseous NH_3 and HNO_2 were calculated through Beer's law only, using the absorbance cross-section reported by Barney et al.[41] Details on the experimental procedure and data processing can be found in Section S3 and Figure S3.

OES Analysis of the Plasma-Produced Species. The NO ($A^2\Sigma^+ - {}^2\Pi$; 226.94 nm), NH ($A^3\Pi - X^3\Sigma$; 336.0 nm), and N_2 ($C^3\Pi - B^3\Pi$; Second Positive System; 337 nm) transitions[42] were measured as shown in Figure S4 (Section S4). We performed measurements (i) axially in the plasma (Figure S4a) as well (ii) space-resolved perpendicularly to the plasma effluent (Figure S4b) using (i) a Horiba iHR550 spectrometer with UV 250 nm blazed grating of 2400 g/mm and (ii) a Zolix Omni750 spectrometer with 500 nm blazed grating of 3600 g/mm equipped with a linear fiber optics array slit, respectively. In the axial position, the presented results were corrected for quenching by H_2O, O_2, and N_2, the sensitivity at different wavelengths, and the difference in the electron impact excitation coefficients for the NO($A^2\Sigma^+$) and NH($A^3\Pi$) states. This means that the intensities of NO($A^2\Sigma^+$) and NH($A^3\Pi$) bands at different gas mixtures can be compared directly after the performed calculations, i.e., as a function of the humidity. The measured intensities can be correlated to ground state NH and NO densities when assuming that excitation to these states occurs predominantly through electron impact. This approach is based on the following approximations (similar to corona approximation[43]): (1) we do not consider collisional excitations, e.g., $N_2(A^3\Sigma)$ + NO → N_2 + NO($A^2\Sigma$); (2)

https://doi.org/10.1021/acssuschemeng.3c00208
ACS Sustainable Chem. Eng. 2023, 11, 4289−4298

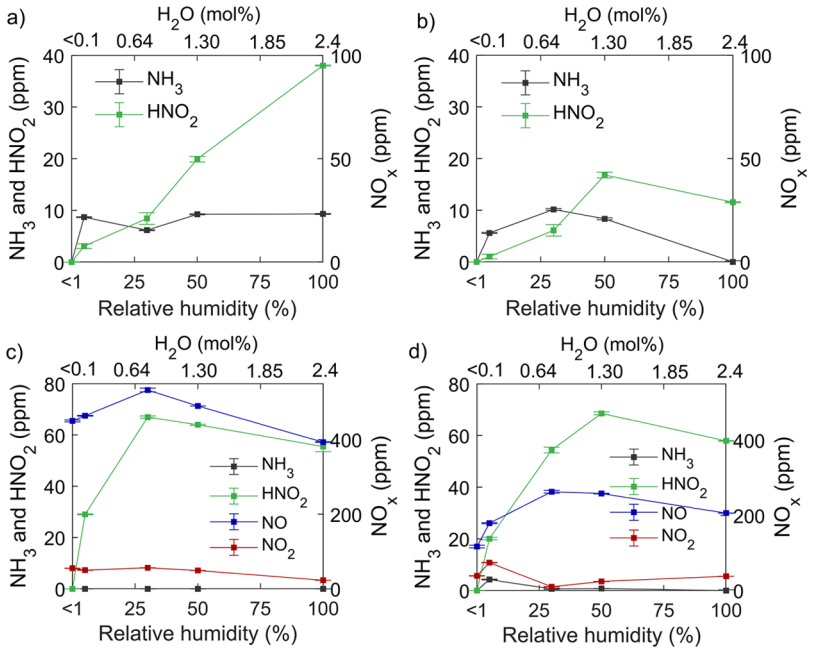

Figure 2. Concentration of NH_3 and HNO_2 (left *y*-axis) and NO_x (right *y*-axis) in the gas phase as a function of feed gas humidity. (a) N_2, 0.5 L/min; (b) N_2, 2 L/min; (c) air, 0.5 L/min; (d) air, 2 L/min.

Table 1. Relevant Reactions, Corresponding Reaction Rate Coefficients, and Relevant Temperature Ranges for the Formation and Decomposition of NH_4NO_x[a]

reaction	rate coefficient[b]/equilibrium constant (R9)[c]	temperature range		ref
$NO + OH + M \rightarrow HNO_2 + M$	$7.52 \times 10^{-31}\ (T/300)^{-2.4}$	200–400 K	R1	59
$NO_2 + OH + M \rightarrow HNO_3 + M$	$1.63 \times 10^{-30}\ (T/300)^{-2.9}$	300–600 K	R2	60
$HNO_2 + NH_3 \rightarrow [NH_4NO_2]$	3.65×10^{-18}	298 K	R3	61
$HNO_2 + NH_4NO_3 \rightarrow [NH_4NO_2] + HNO_3$	n/a		R3	53
$[NH_4NO_2] \rightarrow N_2 + 2H_2O$	n/a (unstable)	<400 K	R5	54
$NH_3(g) + HNO_3(g) \leftrightarrow NH_4NO_3(s)$	$2.46 \times 10^{10} \times (118.87 - 24084/T - 6.025 \times \ln(T))$	265–305 K	R6	62
$NH_4NO_3 \rightarrow N_2O + 2H_2O$[d]	$10^{6.7} \times e^{-86/RT}$, $10^{14} \times e^{-207/RT}$	350–600 K	R7	63
$NH_4NO_3 + NO \rightarrow NO_2 + NH_4NO_2$	n/a		R8	53, 64

[a]M is any neutral molecule and *T* is the gas temperature. [b]Unit: $cm^3/(molecules \times s)$ for two-body reactions and $cm^6/(molecules^2 \times s)$ for three-body reactions. [c]Unit: $molecules^2/cm^6$. [d]In the temperature range 530–560 K, 98% of the irreversible decomposition of NH_4NO_3 occurs via this reaction.[65] However, in NO rich conditions, R8 is more favorable.[53]

the difference in excitation probability is calculated assuming a Maxwell electron energy distribution; (3) we do not consider de-excitation processes through V–V and V–T transfer and charge exchange. We infer that the corrections we made suffice to support the discussion of the obtained results.

The detailed description of the approach, including all computational corrections and normalization based on both experimental data and calculated values can be found in Section S5, Tables S1 and S2.

RESULTS AND DISCUSSION

Net Production of NH_3, NO_x, and HNO_x Downstream.

First, we studied the production of various stable compounds in the gas phase using FTIR, using the setup shown in Figure 1, without base washer, hence following line A. Figure 2a,b shows the NH_3 and HNO_2 concentration in N_2 at 0.5 and 2 L/min gas flow rate. The results of similar experiments, but with humid air, are shown in Figure 2c,d, where besides NH_3 and HNO_2 also NO and NO_2 were detected. At all conditions tested, the N_2O_5, NO_3, O_3, and HNO_3 concentrations were below the limit of detection. The highest observed N_2O concentration did not exceed 2 ppm and was thus considered negligible. An overview of the FTIR bands of interest is presented in Figure S3.

In this discussion, we focus on the possible pathways of nitrogen fixation, leading to the production of HNO_2, HNO_3, and NH_3. A discussion on the NO and NO_2 production and their interplay with water can be found in the Supporting Information.

As a common trend in both humid N_2 and humid air, when the H_2O content of the feed gas increases, the HNO_2 concentration initially rises, as more H and O become available through H_2O dissociation into H atoms and OH radicals. In N_2 feed gas, since NO is produced predominantly from OH (formed through water dissociation), we observe a continuous increase in HNO_2 concentration with increasing humidity, for 0.5 L/min (Figure 2a), while at 2 L/min, a maximum is reached at 50% relative humidity (Figure 2b). In air, the highest HNO_2 concentration (around 70 ppm) is measured between 25% and 50% relative humidity (Figure 2c,d). Note that the chemistry of the system becomes more complex in humid air compared to humid N_2, rendering a detailed discussion on the mechanisms too speculative. However, a plausible hypothesis of why in both N_2 and air,

https://doi.org/10.1021/acssuschemeng.3c00208
ACS Sustainable Chem. Eng. 2023, 11, 4289–4298

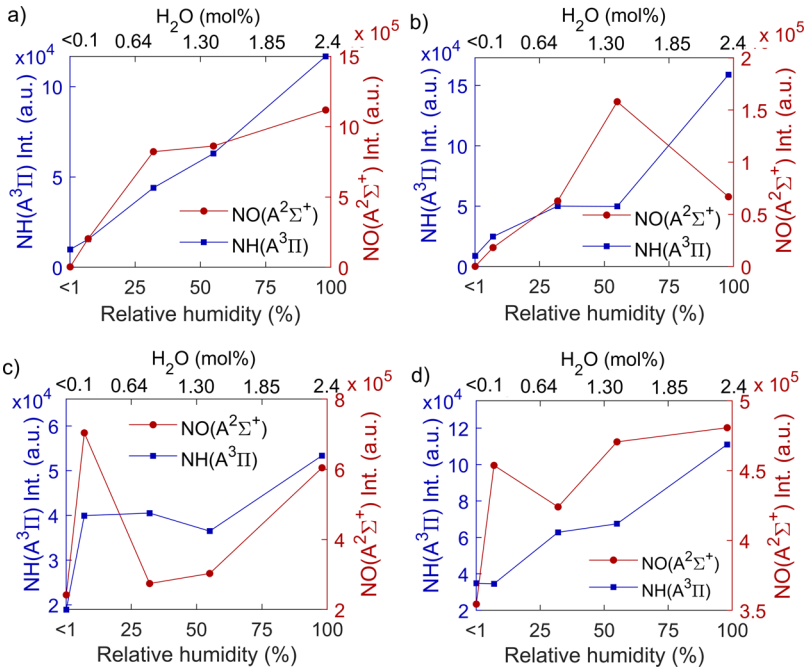

Figure 3. NH($A^3\Pi$) (left *y*-axis) and NO($A^2\Sigma^+$) (right *y*-axis) intensities in the plasma as a function of feed gas humidity. (a) N_2, 0.5 L/min; (b) N_2, 2 L/min; (c) air, 0.5 L/min; (d) air, 2 L/min.

instead of HNO_2 rising until 100% humidity, its concentration decreases at higher H_2O vapor content (i.e., 50−100% for 2 L/min in air and N_2 and 25−100% for 0.5 L/min in air) will be given further down below.

Because H_2O is the sole H source in humid N_2, one could expect the NH_3 concentration to rise with increasing H_2O vapor content as well. However, in the present study, the gas phase NH_3 concentration instead stays constant around 10 ppm at humidity above 5% (N_2, 0.5 L/min; Figure 2a) or even starts dropping after reaching a maximum of ca. 10 ppm at 25% humidity (N_2, 2 L/min; Figure 2b). At the same time, in air, despite H_2O being present as an H source, no NH_3 is detected, except for one condition (air, 2 L/min, 5% humidity; Figure 2d). This is counterintuitive, because we previously observed NH_3 accumulation in liquid when the plasma effluent was placed above a water surface, and NH_3 was measured in PTW (as NH_4^+).[32] Additionally, we confirmed in our previous work that most H in the formed NH_3 came from the gaseous H_2O, with only a minor contribution of liquid H_2O to the formation of NH_3. This clearly indicated that NH_3 should be formed in the gas phase of the plasma system, although it is not detected by the downstream FTIR analysis in the present work. Moreover, HNO_3 (detected in PTW as NO_3^-) was not detected by FTIR in the gas phase under any of the conditions tested. We propose that the reasons are as follows. (i) Gaseous HNO_3 is mainly formed from NO_2 via reaction with OH[36] (see also Table 1 below); however, NO_2 is not detected in humid N_2 (Figure 2a,b), and in humid air, it is present in low concentrations (much lower than NO) (Figure 2c,d). Furthermore, (ii) we hypothesize the formation of NH_4NO_3 and its precipitation out of the gas phase, as described by Zhu et al.[44] The latter hypothesis was supported by the observed accumulation of white dust during our experiments (see below). Still, we need an in situ plasma gas phase analysis to elucidate the presence of NH_x species created by the plasma from N_2 and H_2O in both air and nitrogen feed gas, as shown below.

To investigate the near-simultaneous decrease of NH_3 and HNO_2 at high relative humidity (especially for humid N_2 at 2 L/min; Figure 2b) and the absence of detected NH_3 in air when switching from a humid gas−liquid system (as in our previous work[32]) to a pure humid gas system (Figure 2c,d), we studied the chemical species in the plasma and in the plasma afterglow by means of OES (Figure S4a,b). OES is a widely used analytical technique for qualitative and quantitative plasma analysis. It measures the light emission from state transitions in a nonintrusive way, allowing qualitative insight into (short-lived) species in the plasma itself and right after the plasma, before potential downstream reactions take place.[45]

OES Shows NH and NO Are Produced in the Plasma. First, we analyzed the gas composition immediately inside the plasma. This was done by placing the OES spectrometer axially to the plasma jet (see Figure S4a).

The direct OES data provides the intensity of the signals related to the density of excited species. After the made corrections (described above and in Section S5), we can correlate the intensity of the bands of the excited states NH($A^3\Pi$) and NO($A^2\Sigma^+$) to their ground state density taking into account the approximations behind the corona model applied. This means the resulting corrected data in Figure 3 are representative of the NH and NO ground state concentrations in the plasma. It has been shown that NH is predictive of and correlates with the concentration of NH_3.[46] In (humid) N_2, the trend of NO($A^2\Sigma^+$) intensity follows the gas phase HNO_2 concentration with increasing H_2O content, suggesting NO is directly involved in HNO_2 formation (Figure 3a,b).

On the contrary, in (humid) N_2, the NH trend (based on the NH($A^3\Pi$) intensity) and the NH_3 trend (measured downstream) show opposite behavior at high humidity (50−100% H_2O content; see Figure 2a,b); i.e., inside the plasma, the NH generation continues rising throughout the whole humidity range, corresponding to the increase in H_2O (and hence H), as shown in Figure 3a,b, while NH_3 decreases or plateaus after 50% humidity. Most importantly, the results with

https://doi.org/10.1021/acssuschemeng.3c00208
ACS Sustainable Chem. Eng. 2023, 11, 4289−4298

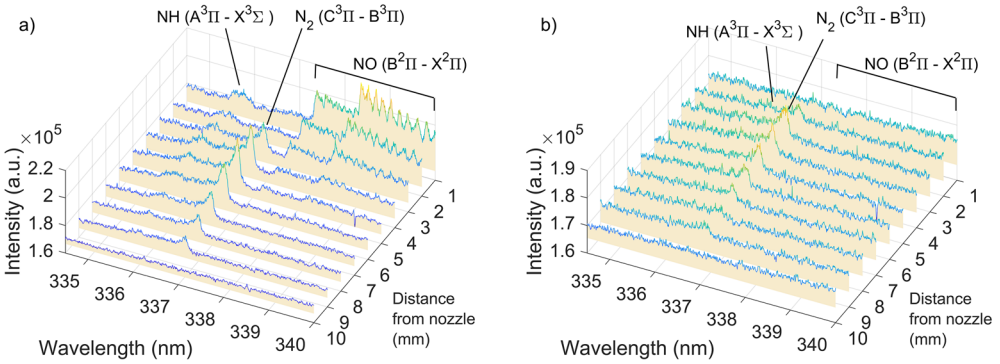

Figure 4. Emission spectra (334−340 nm) as a function of distance from the jet nozzle (1−10 mm) for 5% relative humidity at 2 L/min in N_2 (a) and air (b).

(humid) air not only show the presence of NH($A^3\Pi$) but also its increase with increasing H_2O vapor content (Figure 3c,d), contrary to the lack of NH_3 in the gas phase downstream (see Figure 2c,d). This clearly demonstrates that the NH_3 precursor NH is produced in the plasma, both in humid N_2 and air. This discrepancy in the NH behavior compared to NH_3 suggests that NH_3 is "lost" after the plasma, before the downstream FTIR analysis. In order to obtain insights in the aforementioned pathway of NH_3 decomposition, we used spatially resolved emission spectroscopy, perpendicularly to the plasma effluent (Figure S4b). For these conditions, we also measured $N_2(C^3\Pi-B^3\Pi)$ (see below) and found a correlation between NO and the excited state of N_2. Indeed, next to ground state and vibrationally excited N_2, electronically excited N_2 also plays a role in the main formation reactions of NO, i.e., the Zeldovich mechanism (RS1 and RS2 in the Supporting Information).[35]

NH Presence in the Plasma Afterglow. In the afterglow, the following state transitions were observed: NH($A^3\Pi-X^3\Sigma$), $N_2(C^3\Pi-B^3\Pi)$, and NO($B^2\Pi-X^2\Pi$). The NO($A^2\Sigma^+-X^2\Pi$) transition was below the limit of detection in the afterglow under the conditions studied; however, the NO($B^2\Pi-X^2\Pi$) transition is visible in the 338−340 nm region for some conditions. Figure 4 shows typical emission spectra (334−340 nm) along the plasma jet stream measured at the distance from 1 to 10 mm from the jet's outlet (or nozzle) for 5% relative humidity in N_2 and air at 2 L/min. Spectra for all other conditions (N_2 and air, 0.5 and 2 L/min, from <1 to 100% relative humidity) are found in Figure S5.

It is worth noting that $N_2(C^3\Pi-B^3\Pi)$ was also observed in the axial OES. However, there its presence is noninformative. In contrast, the space-resolved perpendicular OES allowed us to draw conclusions on the relationship between various chemical species present in the plasma afterglow.

While no direct correlation between NO($B^2\Pi-X^2\Pi$) and either of the NH($A^3\Pi$) and $N_2(C^3\Pi)$ was found, the obtained data allowed us to draw conclusions on the relationship between NH($A^3\Pi$) and $N_2(C^3\Pi)$. At all conditions, NH($A^3\Pi$) correlates strongly with the presence of $N_2(C^3\Pi)$ in the plasma and in the afterglow. Indeed, next to vibrationally excited N_2, electronically excited N_2 also plays a role in the splitting of N_2, which is a necessary step in NH formation.[35] Interestingly, at low humidity (5−30%) in N_2, another excited state, $N_2(B^2\Pi)$, is formed through high energy electrons and is effectively quenched at higher H_2O concentrations and at higher O_2 fractions.[47] This is the reason the NO($B^2\Pi$) emission is visible only in N_2 gas and only at low humidity (Figure 4a; see also Figure S5k,q and to a lesser extent panels l and r). NH($A^3\Pi$) is observed in N_2 even when only trace amounts of H_2O vapor are present (see Figures S5k and S4p), due to the relatively low excitation energy needed for NH ground state excitation (3.68 eV)[48] and because there is only a small amount of strong quenchers present (i.e., H_2O) for NH($A^3\Pi$)[49,50] in the feed gas.

As discussed above, no NH_3 was detected in the gas phase downstream when humid air was used as feed gas. At the same time, we have measured NH_3 in liquid when the plasma was placed above liquid water[32] and we observe by OES the formation of NH($A^3\Pi$), an indicator for NH_3, when humid air is used, both in the plasma and in the afterglow.

NH_3 and HNO_x Loss through Salt Formation and Decomposition. To explain this discrepancy, we considered that NH_3 can form salts with HNO_x and looked at the most commonly reported pathways for the formation and decomposition of NH_4NO_x (summarized in Table 1, R1−R8).[51−53] It is known from a selective catalytic reduction process (SCR) that NO_x and HNO_x can react with NH_3, which facilitates their conversion into N_2 and H_2O via NH_4NO_2 and NH_4NO_3 intermediates. Unlike in SCR, in plasma synthesis, the formation of NH_4NO_2 is undesirable as it decomposes back to N_2 and H_2O at room temperature and atmospheric pressure.[54] On the other hand, NH_4NO_3 is more stable and requires higher temperatures to undergo decomposition (R7).[52,55,56] The formation of NH_4NO_x has been observed in plasma systems as well, e.g., in dielectric barrier discharge (DBD) plasmas which focus on NH_3 oxidation.[57,58]

In our experimental setup, the residence time between the plasma and the FTIR (0.07 and 0.3 s for 2 and 0.5 L/min, respectively) is sufficient to allow complete conversion of NH_3 and HNO_2 into NH_4NO_2 (assuming reaction R3). Indeed, the time scale for loss of NH_3 (drop in concentration from 50 to 0.1 ppm) would be around 0.1 s, making NH_4NO_2 formation a plausible pathway in this system.

Therefore, we hypothesize that downstream from the plasma in our system HNO_2 reacts with NH_3 to form NH_4NO_2, which rapidly decomposes into N_2 and H_2O (R3−R5).[55,66] We note that NH_4NO_2 can also be formed through HNO_3 as an intermediate (R4). However, we assume this pathway to be negligible in our experiments because we observe HNO_3 neither in the gas nor in the liquid.

Another plausible explanation is the precipitation of NH_4NO_3, which has also been described in SCR systems and as a direct product in plasma systems.[52,55,56] However, in the case of N_2 as feed gas, formation of NH_4NO_3 is unlikely:

https://doi.org/10.1021/acssuschemeng.3c00208
ACS Sustainable Chem. Eng. 2023, 11, 4289−4298

this would require HNO_3 being present, but we detected HNO_3 neither in the gas phase (this work) nor in PTW in our previous work.[32] Therefore, we infer that, while in humid air plasma the loss of NH_3 is possible through NH_4NO_3 (R6, R7 and R8) and NH_4NO_2 (R3, R4, R5 and R8), in N_2 plasma the loss of NH_3 at higher humidity levels, as seen in Figure 2a,b, occurs almost solely through NH_4NO_2.

To confirm our hypothesis about NH_4NO_x, we performed an in-line removal of HNO_2 (and possibly HNO_3) immediately after plasma by adding a Drechsel flask with a 1 M aqueous solution of NaOH (see Figure 1, following line B, i.e., including the base washer). This basic medium completely dissolves gaseous HNO_x, while hindering the solvation of gaseous NH_3 which thus passes further downstream, as was shown in the case of N_2 with H_2O vapor.[23] Figure 5 shows the

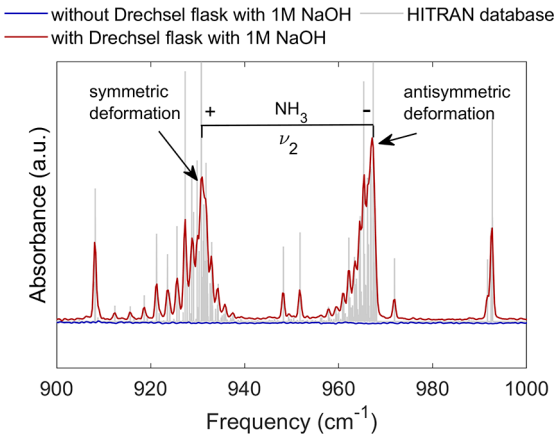

Figure 5. FTIR spectra of the NH_3 ν_2 deformation region, with and without HNO_x removal by NaOH, at 100% relative humidity in air, 2 L/min. The symmetric and antisymmetric deformations of NH_3 are shown, together with the simulated NH_3 spectrum in this range as obtained from the HITRAN database.[67]

effect of HNO_x removal on the FTIR spectra, reflected in the NH_3 concentration measured in the gas phase downstream from plasma. When an alkaline medium is added to trap HNO_2, the concentration of NH_3 in humid air goes from nondetectable (cf. also Figure 2c,d) to clearly detectable (Figure 5). Specifically, at 2 L/min air and 100% RH, we measured NH_3 concentration of ca. 50 ppm in the gas phase. This fully supports our above hypothesis.

Thus, we demonstrate for the first time that NF from air with H_2O vapor proceeds via a pathway toward NH_3 as well as NO_x/HNO_x, but this can be overlooked because of the product loss downstream due to side reactions leading to NH_3 decomposition.

These data are consistent with the drop in HNO_2 and NH_3 concentrations at a H_2O content above 30% relative humidity (Figure 2). Once HNO_2 and NH_3 are produced simultaneously, NH_4NO_2 starts being formed and further decomposes, thus effectively decreasing the net HNO_2 and NH_3 production. In air, the concentrations of the generated HNO_x are certainly higher than in N_2, due to the presence of O_2 and associated oxidative pathways. At the same time, in air the concentration of NH_3 is likely lower due to the larger contribution of competing reactions with the excited N_2 molecules (i.e., oxidative versus reductive NF). As a result, some (but not all) NH_3 and some HNO_x are likely lost due to the NH_4NO_x formation when N_2 is the feed gas, while virtually all NH_3 is lost when using air.

This effect appears to be slightly different at 0.5 L/min in N_2 (Figure 2a). Even though the NH_3 concentration plateaus instead of rises upon increasing humidity, both HNO_2 and NH_3 do not drop (as is the case with other high humidity conditions, Figure 2b,d), and HNO_2 even shows a rising trend until 100% humidity. While the specific reasons for this are unclear at this point, we propose that the adverse effect of NH_4NO_x formation is still present, because otherwise the continuous rise of NH_3 concentrations should be observable. This question presents an important point for further research aimed at decreasing this loss mechanism, next to the use of an in-line HNO_2 removal.

However, as mentioned above, NH_4NO_2 is not the only salt formed from NH_3 and HNO_x. In our experiments, we observed the build-up of a fine white powder in the quartz tube used during the OES experiments, Qualitative analysis of the powder via the indophenol blue reaction (described elsewhere[27,68]) demonstrated that the cation of the salt was indeed NH_4^+.[24,47] Due to the limited availability of analytical equipment, the anion could not be identified, but a negative Griess reagent test[69] excluded the presence of NO_2^-. This is in agreement with NH_4NO_2 not being a stable product at atmospheric pressure and room temperature[54] (see Table 1). Therefore, we conclude that the anion was likely NO_3^-, in agreement with Zhu et al.,[44] who observed NH_4NO_3 dust formation after operating plasma which contained both NH_3 and NO_x. We note, however, that the amount of solid formed after weeks of our experiments (at different flow rates and humidity values) was in the range of mg. This is due to the (likely) very low amount of HNO_3 formed in our plasma.[70] Indeed, although low concentrations of HNO_3 would be expected in our experiments because substantial amounts of NO_2 are produced in the gas phase with air plasma, no HNO_3 was detected. Hence, it is reasonable to conclude that all formed HNO_3 reacted with NH_3 to form NH_4NO_3. Interestingly, when liquid H_2O was used to accumulate the NF products, both NO_3^- and NH_4^+ were detected in PTW with air plasma. In the case of a close liquid surface, NH_4NO_3 did not precipitate out of the gas phase due to the short flight time to the liquid surface. Liquid water prevents decomposition via dissolution; the coordination of ions with water molecules in solution stabilizes the ions and inhibits decomposition reactions.

Furthermore, a semiquantitative assessment of the relative loss pathways in this case was performed with humid air. We performed the experiment with 2 L/min of air and 100% RH for 3 h, during which we observed precipitate deposition on the tubing. After this, a gravimetric analysis of the precipitate was performed by washing the precipitate off the walls of the tubing. After evaporation of water, the mass of the accumulated precipitate was found to be below 5 mg. As shown above, by introducing the alkaline washer, 50 ppm of NH_3 was "recovered" under these conditions (we note once again that the alkaline washer is not selective and removes HNO_x rather than only HNO_2 or only HNO_3). This amounts to ca. 74 nmol/s of NH_3. From the stoichiometry of NH_4NO_3 formation, we conclude that after 3 h the amount of precipitate would constitute 64 mg if all of it was NH_4NO_3, which is not the case. Thus, the relative contribution of the NH_4NO_3 pathway to NH_3 loss does not exceed 10%. Therefore, even

https://doi.org/10.1021/acssuschemeng.3c00208
ACS Sustainable Chem. Eng. 2023, 11, 4289−4298

in the humid air plasma, most of NH_3 is lost via the generation and subsequent decomposition of NH_4NO_2.

Although performance optimization is not the focus of this work, we also assessed the energy consumption (EC) and the production rate (PR) of NF in our experiments. The EC and PR values and the calculation method are presented in the Supporting Information; see Tables S5 and S6. The data presented in Table S6 demonstrates that numerical values of PR are different for different conditions, as follows from the different selectivity toward different products (see Figure 2 above). For example, at 2 L/min of N_2 and 100% relative humidity, the main product is HNO_2 (with a PR of 2.9 mg/h). Under the same conditions but in air, NO is the main product (with a PR of 29 mg/h). The relative improvement in a hypothetical scenario when NH_3 and HNO_2/HNO_3 are not lost in our experiments was evaluated. Let us consider example conditions of humid air plasma operated at 2 L/min and 100% RH, i.e., the same conditions at which the experiment with the HNO_x-removing washer was performed. Here, we detect 50 ppm of NH_3, which means also 50 ppm of HNO_x was lost. The overall concentration of NF products without accounting for the NH_4NO_x loss is ca. 300 ppm (see Figure 2d), which becomes 400 ppm when NH_4NO_x is not lost. Therefore, the relative decrease in EC and the relative increase in PR when the product loss is avoided amount to ca. 30%. Using liquid water as a reservoir to accumulate the nitrogen fixation products can aid in this. Taken together, these data clearly suggest that using liquid H_2O in proximity to the plasma zone is beneficial: it increases the total net accumulation of the NF products, because it reduces or even eliminates the loss of NH_4NO_x.

CONCLUSIONS

We studied the pathways of nitrogen fixation in humid N_2 and humid air plasma using optical emission spectroscopy and Fourier-transform infrared spectroscopy. We revealed that the increased NH emission as well as NH ground state density strongly correlate with the water vapor content in both N_2 and air plasmas, indicating that the reduction nitrogen fixation pathway (toward NH_3 formation) takes place in both gas mixtures.

We show for the first time that NH_3 is produced in air plasma in non-negligible quantities (in the same order of magnitude as HNO_2 and only an order of magnitude lower than NO and NO_2 combined). However, in both air and N_2, this nitrogen fixation pathway is strongly affected by the presence of HNO_2 and HNO_3.

In humid air, the formation of both NH_4NO_3 and NH_4NO_2 likely occurs. Although both of these can decrease the process efficiency downstream, part of NH_3 remains in a fixated form as precipitated NH_4NO_3. In contrast, in humid N_2, we ascribe the loss pathway exclusively to NH_4NO_2, which is unstable and decomposes to N_2 and H_2O, decreasing the overall nitrogen fixation efficiency.

In summary, our work shows that (1) the selectivity of nitrogen fixation in air and N_2 plasmas can be controlled by changing the humidity of the feed gas, (2) NH_3 production can be achieved in both N_2 and air plasma using H_2O as a hydrogen source, and (3) the adverse effects of NH_4NO_2 formation hinder the net production and, therefore, the overall efficiency of the plasma-based nitrogen fixation process. The latter means that, under conditions where HNO_2 and NH_3 are produced simultaneously, it is important to suppress the reverse process (via decomposition of NH_4NO_2). This can be performed through an in-line removal of HNO_2 from the gas mixture or by using plasma-treated water to accumulate all nitrogen fixated products simultaneously without losses.

ASSOCIATED CONTENT

Supporting Information

The Supporting Information is available free of charge at https://pubs.acs.org/doi/10.1021/acssuschemeng.3c00208.

Additional details on the experimental setup of optical analyses, calculational methodology for OES and FTIR, and further experimental data (PDF)

AUTHOR INFORMATION

Corresponding Author

Elise Vervloessem − *Research group PLASMANT, Department of Chemistry, University of Antwerp, 2610 Wilrijk, Belgium; Research Unit Plasma Technology (RUPT), Department of Applied Physics, Ghent University, 9000 Ghent, Belgium;* orcid.org/0000-0003-0412-7597; Email: elise.vervloessem@uantwerpen.be

Authors

Mikhail Gromov − *Research Unit Plasma Technology (RUPT), Department of Applied Physics, Ghent University, 9000 Ghent, Belgium; Chimie des Interactions Plasma Surface (ChiPS), CIRMAP, Mons University, 7000 Mons, Belgium;* orcid.org/0000-0002-6543-8914

Nathalie De Geyter − *Research Unit Plasma Technology (RUPT), Department of Applied Physics, Ghent University, 9000 Ghent, Belgium*

Annemie Bogaerts − *Research group PLASMANT, Department of Chemistry, University of Antwerp, 2610 Wilrijk, Belgium;* orcid.org/0000-0001-9875-6460

Yury Gorbanev − *Research group PLASMANT, Department of Chemistry, University of Antwerp, 2610 Wilrijk, Belgium;* orcid.org/0000-0002-8059-4464

Anton Nikiforov − *Research Unit Plasma Technology (RUPT), Department of Applied Physics, Ghent University, 9000 Ghent, Belgium;* orcid.org/0000-0002-2255-6419

Complete contact information is available at: https://pubs.acs.org/10.1021/acssuschemeng.3c00208

Author Contributions

‖Y.G. and A.N. contributed equally.

Funding

This research is supported by the Excellence of Science FWO-FNRS project (NITROPLASM, FWO grant ID GoF9618n, EOS ID 30505023), the European Research Council (ERC) under the European Union's Horizon 2020 research and innovation program (grant No. 810182 − SCOPE ERC Synergy project), and the Fund for Scientific Research (FWO) Flanders Bioeconomy project (grant No. G0G2322N), funded by the European Union-NextGenerationEU.

Notes

The authors declare no competing financial interest.

ACKNOWLEDGMENTS

We would like to thank E. H. Choi and co-workers from the Plasma Bioscience Research Center (Republic of Korea) for providing the plasma jet used in this work.

ABBREVIATIONS

HB, Haber-Bosch; NF, nitrogen fixation; PTW, plasma-treated water; UV, ultraviolet; EC, energy consumption; FTIR, Fourier transform infrared spectroscopy; OES, optical emission spectroscopy; MFC, mass flow controller; Ls, standard liter

REFERENCES

(1) Smil, V. Nitrogen and Food Production: Proteins for Human Diets. *Ambio* **2002**, *31* (2), 126−131.

(2) Appl, M. Ammonia, 2. Production Processes. In *Ullmann's Encyclopedia of Industrial Chemistry*; Wiley-VCH Verlag GmbH & Co. KGaA, 2011.

(3) Erisman, J. W.; Sutton, M.; Galloway, J.; Klimont, Z.; Winiwarter, W. How a Century of Ammonia Synthesis Changed the World. *Nat. GeoSci.* **2008**, *1* (10), 636−639.

(4) Nayak-Luke, R. M.; Banares-Alcantara, R. Techno-Economic Viability of Islanded Green Ammonia as a Carbon-Free Energy Vector and as a Substitute for Conventional Production. *Energy Environ. Sci.* **2020**, *13*, 2957−2966.

(5) Bicer, Y.; Dincer, I.; Zamfirescu, C.; Vezina, G.; Raso, F. Comparative Life Cycle Assessment of Various Ammonia Production Methods. *J. Clean. Prod.* **2016**, *135*, 1379−1395.

(6) Cherkasov, N.; Ibhadon, A. O.; Fitzpatrick, P. A Review of the Existing and Alternative Methods for Greener Nitrogen Fixation. *Chem. Eng. Process.* **2015**, *90*, 24−33.

(7) Anastasopoulou, A.; Butala, S.; Lang, J.; Hessel, V.; Wang, Q. Life Cycle Assessment of the Nitrogen Fixation Process Assisted by Plasma Technology and Incorporating Renewable Energy. *Ind. Eng. Chem. Res.* **2016**, *55*, 8141−8153.

(8) Hochman, G.; Goldman, A. S.; Felder, F. A.; Mayer, J. M.; Miller, A. J. M.; Holland, P. L.; Goldman, L. A.; Manocha, P.; Song, Z.; Aleti, S. Potential Economic Feasibility of Direct Electrochemical Nitrogen Reduction as a Route to Ammonia. *ACS Sust. Chem. Eng.* **2020**, *8* (24), 8938−8948.

(9) Bogaerts, A.; Neyts, E. C. Plasma Technology: An Emerging Technology for Energy Storage. *ACS Energy Lett.* **2018**, *3* (4), 1013−1027.

(10) Winter, L. R.; Chen, J. G. N2 Fixation by Plasma-Activated Processes. *Joule* **2021**, *5* (2), 300−315.

(11) Patil, B. S.; Wang, Q.; Hessel, V.; Lang, J. Plasma N 2 -Fixation : 1900 − 2014. *Catal* **2015**, *256*, 49−66.

(12) Vervloessem, E.; Aghaei, M.; Jardali, F.; Hafezkhiabani, N.; Bogaerts, A. Plasma-Based N2Fixation into NOx: Insights from Modeling toward Optimum Yields and Energy Costs in a Gliding Arc Plasmatron. *ACS Sustain. Chem. Eng.* **2020**, *8* (26), 9711−9720.

(13) Jardali, F.; van Alphen, S.; Creel, J.; Ahmadi Eshtehardi, H.; Axelsson, M.; Ingels, R.; Snyders, R.; Bogaerts, A. NO x Production in a Rotating Gliding Arc Plasma: Potential Avenue for Sustainable Nitrogen Fixation. *Green Chem.* **2021**, *23*, 1748−1757.

(14) Kelly, S.; Bogaerts, A. Nitrogen Fixation in an Electrode-Free Microwave Plasma. *Joule* **2021**, *5* (11), 3006−3030.

(15) van Alphen, S.; Ahmadi Eshtehardi, H.; O'Modhrain, C.; Bogaerts, J.; van Poyer, H.; Creel, J.; Delplancke, M. P.; Snyders, R.; Bogaerts, A. Effusion Nozzle for Energy-Efficient NOx Production in a Rotating Gliding Arc Plasma Reactor. *Chem. Eng. J.* **2022**, *443*, 136529−136541.

(16) Rouwenhorst, K. H. R.; Engelmann, Y.; van 'T Veer, K.; Postma, R. S.; Bogaerts, A.; Lefferts, L. Plasma-Driven Catalysis: Green Ammonia Synthesis with Intermittent Electricity. *Green Chem.* **2020**, *22* (19), 6258−6287.

(17) Carreon, M. L. Plasma Catalytic Ammonia Synthesis : State of the Art and Future Directions. *J. Phys. D: Appl. Phys.* **2019**, *52*, 483001−483025.

(18) Huang, Z.; Xiao, A.; Liu, D.; Lu, X.; Ostrikov, K. Plasma-Water-Based Nitrogen Fixation: Status, Mechanisms, and Opportunities. *Plasma Processes Polym.* **2022**, *19* (4), 2100198−2100211.

(19) Chehade, G.; Dincer, I. Progress in Green Ammonia Production as Potential Carbon-Free Fuel. *Fuel* **2021**, *299*, 120845−120879.

(20) Peng, P.; Chen, P.; Addy, M.; Cheng, Y.; Zhang, Y.; Anderson, E.; Zhou, N.; Schiappacasse, C.; Hatzenbeller, R. In Situ Plasma-Assisted Atmospheric Nitrogen Fixation Using Water and Spray-Type Jet Plasma†. *Chem. Commun.* **2018**, *54*, 2886−2889.

(21) Peng, P.; Schiappacasse, C.; Zhou, N.; Addy, M.; Cheng, Y.; Zhang, Y.; Anderson, E.; Chen, D.; Wang, Y.; Liu, Y.; Chen, P.; Ruan, R. Plasma in Situ Gas-Liquid Nitrogen Fixation Using Concentrated High-Intensity Electric Field. *J. Phys. D: Appl. Phys.* **2019**, *52* (49), 494001−494009.

(22) Kumari, S.; Pishgar, S.; Schwarting, M. E.; Paxton, W. F.; Spurgeon, J. M. Synergistic Plasma-Assisted Electrochemical Reduction of Nitrogen to Ammonia. *Chem. Commun.* **2018**, *54* (95), 13347−13350.

(23) Sakakura, T.; Takatsuji, Y.; Morimoto, M.; Haruyama, T. Nitrogen Fixation through the Plasma/Liquid Interfacial Reaction with Controlled Conditions of Each Phase as the Reaction Locus. *Electrochemistry* **2020**, *88* (3), 190−194.

(24) Sakakura, T.; Murakami, N.; Takatsuji, Y.; Haruyama, T. Nitrogen Fixation in a Plasma/Liquid Interfacial Reaction and Its Switching between Reduction and Oxidation. *J. Phys. Chem. C* **2020**, *124* (17), 9401−9408.

(25) Sakakura, T.; Murakami, N.; Takatsuji, Y.; Morimoto, M.; Haruyama, T. Contribution of Discharge Excited Atomic N, N2*, and N2+ to a Plasma/Liquid Interfacial Reaction as Suggested by Quantitative Analysis. *ChemPhysChem* **2019**, *20* (11), 1467−1474.

(26) Sakakura, T.; Uemura, S.; Hino, M.; Kiyomatsu, S.; Takatsuji, Y.; Yamasaki, R.; Morimoto, M.; Haruyama, T. Excitation of H2O at the Plasma/Water Interface by UV Irradiation for the Elevation of Ammonia Production. *Green Chem.* **2018**, *20* (3), 627−633.

(27) Haruyama, T.; Namise, T.; Shimoshimizu, N.; Uemura, S.; Takatsuji, Y.; Hino, M.; Yamasaki, R.; Kamachi, T.; Kohno, M. Non-Catalyzed One-Step Synthesis of Ammonia from Atmospheric Air and Water. *Green Chem.* **2016**, *18* (16), 4536−4541.

(28) Sun, J.; Alam, D.; Daiyan, R.; Masood, H.; Zhang, T.; Zhou, R.; Cullen, P. J.; Lovell, E. C.; Jalili, A. R.; Amal, R. A Hybrid Plasma Electrocatalytic Process for Sustainable Ammonia Production. *Energy Environ. Sci.* **2021**, *14*, 865−872.

(29) Hawtof, R.; Ghosh, S.; Guarr, E.; Xu, C.; Sankaran, R. M.; Renner, J. N. Catalyst-Free, Highly Selective Synthesis of Ammonia from Nitrogen and Water by a Plasma Electrolytic System. *Sci. Adv.* **2019**, *5* (1), eaat5778−9.

(30) Sharma, R. K.; Patel, H.; Mushtaq, U.; Kyriakou, V.; Zafeiropoulos, G.; Peeters, F.; Welzel, S.; van de Sanden, M. C. M.; Tsampas, M. N. Plasma Activated Electrochemical Ammonia Synthesis from Nitrogen and Water. *ACS Energy Lett.* **2021**, *6* (2), 313−319.

(31) Chen, H.; Yuan, D.; Wu, A.; Lin, X.; Li, X. Review of Low-Temperature Plasma Nitrogen Fixation Technology. *Waste Disposal and Sustainable Energy* **2021**, *3*, 201−217.

(32) Gorbanev, Y.; Vervloessem, E.; Nikiforov, A.; Bogaerts, A. Nitrogen Fixation with Water Vapor by Nonequilibrium Plasma: Toward Sustainable Ammonia Production. *ACS Sust. Chem. Eng.* **2020**, *8*, 2996−3004.

(33) Zhang, T.; Zhou, R.; Zhang, S.; Zhou, R.; Ding, J.; Li, F.; Hong, J.; Dou, L.; Shao, T.; Murphy, A. B.; Ostrikov, K.; Cullen, P. J. Sustainable Ammonia Synthesis from Nitrogen and Water by One-Step Plasma Catalysis. *Energy Environ. Mater.* **2022**, DOI: 10.1002/eem2.12344.

(34) Rouwenhorst, K. H. R.; Jardali, F.; Bogaerts, A.; Lefferts, L. From the Birkeland-Eyde Process towards Energy-Efficient Plasma-Based NOX Synthesis: A Techno- Economic Analysis. *Energy Environ. Sci.* **2021**, *14*, 2520−2534.

(35) Vervloessem, E.; Gorbanev, Y.; Nikiforov, A.; de Geyter, N.; Bogaerts, A. Sustainable NOx Production from Air in Pulsed Plasma: Elucidating the Chemistry behind the Low Energy Consumption. *Green Chem.* **2022**, *24*, 916−929.

https://doi.org/10.1021/acssuschemeng.3c00208
ACS Sustainable Chem. Eng. 2023, 11, 4289−4298

(36) Hollevoet, L.; Vervloessem, E.; Gorbanev, Y.; Nikiforov, A.; de Geyter, N.; Bogaerts, A.; Martens, J. A. Energy-Efficient Small-Scale Ammonia Synthesis Process with Plasma-Enabled Nitrogen Oxidation and Catalytic Reduction of Adsorbed NOx. *ChemSusChem* **2022**, *15* (10), e202102526.
(37) Toth, J. R.; Abuyazid, N. H.; Lacks, D. J.; Renner, J. N.; Sankaran, R. M. A Plasma-Water Droplet Reactor for Process-Intensified, Continuous Nitrogen Fixation at Atmospheric Pressure. *ACS Sust. Chem. Eng.* **2020**, *8* (39), 14845−14854.
(38) Gorbanev, Y.; Verlackt, C. C. W.; Tinck, S.; Tuenter, E.; Foubert, K.; Cos, P.; Bogaerts, A. Combining Experimental and Modelling Approaches to Study the Sources of Reactive Species Induced in Water by the COST RF Plasma Jet. *Phys. Chem. Chem. Phys.* **2018**, *20* (4), 2797−2808.
(39) Gorbanev, Y.; O'Connell, D.; Chechik, V. Non-Thermal Plasma in Contact with Water: The Origin of Species. *Chem.—Eur. J.* **2016**, *22* (10), 3496−3505.
(40) Gordon, I. E.; Rothman, L. S.; Hargreaves, R. J.; Hashemi, R.; Karlovets, E. V.; Skinner, F. M.; Conway, E. K.; Hill, C.; Kochanov, R. V.; Tan, Y.; Wcisło, P.; Finenko, A. A.; Nelson, K.; Bernath, P. F.; Birk, M.; Boudon, V.; Campargue, A.; Chance, K. V.; Coustenis, S. N. The HITRAN2020 Molecular Spectroscopic Database. *J. Quant. Spectrosc. Radiat. Transfer* **2022**, *277*, 107949.
(41) Barney, W. S.; Wingen, L. M.; Lakin, M. J.; Brauers, T.; Stutz, J.; Finlayson-Pitts, B. J. Infrared Absorption Cross-Section Measurements for Nitrous Acid (HONO) at Room Temperature. *J. Phys. Chem. A* **2000**, *104* (8), 1692−1699.
(42) Pearse, R. W. B.; Gaydon, A. G. *Identification of Molecular Spectra*, Second Edition; Chapman & Hall LTD: London, 1950; 276 pp.
(43) Lieberman, M. A.; Lichtenberg, A. J. *Principles of Plasma Discharges and Plasma Materials Processing*, second, ed.; John Wiley & Sons: Hoboken, NJ, 2005; 575 pp.
(44) Zhu, Y.; Xiong, Z.; Li, M.; Chen, X.; Lu, C. Investigation of NH 4 NO 3 Formation by Air Plasma and Wasted Ammonia. *Plasma Process Polym.* **2021**, *18* (8), 2000223.
(45) Bruggeman, P.; Brandenburg, R. Atmospheric Pressure Discharge Filaments and Microplasmas: Physics, Chemistry and Diagnostics. *J. Phys. D: Appl. Phys.* **2013**, *46* (46), 464001−464029.
(46) van Duc Long, N.; Al-Bared, M.; Lin, L.; Davey, K.; Tran, N. N.; Pourali, N.; Ken Ostrikov, K.; Rebrov, E.; Hessel, V. Understanding Plasma-Assisted Ammonia Synthesis via Crossing Discipline Borders of Literature: A Critical Review. *Chem. Eng. Sci.* **2022**, *263*, 118097−118110.
(47) Liu, Y.; Tan, Z.; Chen, X.; Li, X.; Wang, X. A Numerical Investigation on the Effects of Water Vapor on Electron Energy and Oh Production in Atmospheric-Pressure He/H2o and Ar/H2o Plasma Jets. *IEEE Trans Plasma Sci.* **2019**, *47* (3), 1593−1604.
(48) Mo, Y.; Ottinger, C.; Shen, G. Collision-Induced Intersystem Crossing from NH(A1Δ, b 1Σ+) to NH(A3∏): Gateway-Mediated and Direct Mechanisms. *J. Chem. Phys.* **1999**, *111* (10), 4598−4612.
(49) Buckley, S. G.; Damm, C. J.; Vitovec, W. M.; Anne Sgro, L.; Sawyer, R. F.; Koshland, C. P.; Lucas, D. Ammonia Detection and monitoring with Photofragmentation Fluorescence. *Appl. Opt.* **1998**, *37*, 8382−8391.
(50) Hofzumahaus, A.; Stuhl, F. Electronic Quenching, Rotational Relaxation, and Radiative Lifetime of NH(A3Π,V′=0,N′). *J. Chem. Phys.* **1985**, *82* (7), 3152−3159.
(51) Jiang, B.; Zhao, S.; Wang, Y.; Wenren, Y.; Zhu, Z.; Harding, J.; Zhang, X.; Tu, X.; Zhang, X. Plasma-Enhanced Low Temperature NH3-SCR of NOx over a Cu-Mn/SAPO-34 Catalyst under Oxygen-Rich Conditions. *Appl. Catal., B* **2021**, *286*, 119886−119897.
(52) Grossale, A.; Nova, I.; Tronconi, E.; Chatterjee, D.; Weibel, M. The Chemistry of the NO/NO2-NH3 "Fast" SCR Reaction over Fe-ZSM5 Investigated by Transient Reaction Analysis. *J. Catal.* **2008**, *256* (2), 312−322.
(53) Kubota, H.; Liu, C.; Toyao, T.; Maeno, Z.; Ogura, M.; Nakazawa, N.; Inagaki, S.; Kubota, Y.; Shimizu, K.-I. Formation and Reactions of NH4NO3 during Transient and Steady-State NH3-SCR of NOx over H-AFX Zeolites: Spectroscopic and Theoretical Studies. *ACS Catal.* **2020**, *10* (3), 2334−2344.
(54) Mebel, A. M.; Lin, M. C.; Morokuma, K.; Melius, C. F. Theoretical Study of the Gas-Phase Structure, Thermochemistry, and Decomposition Mechanisms of NH4NO2 and NH4(NO2)2. *J. Phys. Chem.* **1995**, *99* (18), 6842−6848.
(55) Sun, Q.; Gao, Z.-X.; Wen, B.; Sachtler, W. M. H. Spectroscopic Evidence for a Nitrite Intermediate in the Catalytic Reduction of NOx with Ammonia on Fe/MFI. *Catal. Lett.* **2002**, *78*, 1−5.
(56) Savara, A.; Li, M. J.; Sachtler, W. M. H.; Weitz, E. Catalytic Reduction of NH4NO3 by NO: Effects of Solid Acids and Implications for Low Temperature DeNOx Processes. *Appl. Catal., B* **2008**, *81* (3−4), 251−257.
(57) Zhang, X.; Zhang, Y.; Lu, H.; Zhu, Z.; Han, J. Characteristics of Ammonia Oxidation in a Dielectric Barrier Discharge Reactor. *IEEE Trans. Plasma Sci.* **2020**, *48* (10), 3616−3620.
(58) Kim, D.-J.; Choi, Y.; Kim, K.-S. Effects of Process Variables on NOx Conversion by Pulsed Corona Discharge Process. *Plasma Chem. Plasma Process.* **2001**, *21* (4), 625−650.
(59) Atkinson, R.; Baulch, D. L.; Cox, R. A.; Crowley, J. N.; Hampson, R. F.; Hynes, R. G.; Jenkin, M. E.; Rossi, M. J.; Troe, J.; Center, P. R.; Science, L. H.; Centre, T.; Park, S. Evaluated Kinetic and Photochemical Data for Atmospheric Chemistry: Volume I − Gas Phase Reactions of Ox, HOx, NOx and SOx Species. *Atmos. Chem. Phys.* **2004**, *4*, 1461−1738.
(60) Hippler, H.; Krasteva, N.; Nasterlack, S.; Striebel, F. Reaction of OH + NO2: High Pressure Experiments and Falloff Analysis †. *J. Phys. Chem. A* **2006**, *110*, 6781−6788.
(61) Pagsberg, P.; Ratajczak, E.; Sillesen, A.; Latajka, Z. Kinetics and Thermochemistry of the Reversible Gas Phase Reaction HONO + NH3 = H3N-HONO Studied by Infrared Diode Laser Spectroscopy. *Chem. Phys. Lett.* **1994**, *227*, 6−12.
(62) Mozurkewich, M. The Dissociation Constant of Ammonium Nitrate and Its Dependence on Temperature, Relative Humidity and Particle Size. *Atmos. Environ.* **1993**, *27* (2), 261−270.
(63) Vyazovkin, S.; Clawson, J. S.; Wight, C. A. Thermal Dissociation Kinetics of Solid and Liquid Ammonium Nitrate. *Chem. Mater.* **2001**, *13* (3), 960−966.
(64) Shan, Y.; Shi, X.; He, G.; Liu, K.; Yan, Z.; Yu, Y.; He, H. Effects of NO2 Addition on the NH3-SCR over Small-Pore Cu−SSZ-13 Zeolites with Varying Cu Loadings. *J. Phys. Chem. C* **2018**, *122* (45), 25948−25953.
(65) Feick, G.; Hainer, R. M. On the Thermal Decomposition of Ammonium Nitrate. Steady-State Reaction Temperatures and Reaction Rate. *J. Am. Chem. Soc.* **1954**, *76*, 5860−5863.
(66) Li, M.; Henao, J.; Yeom, Y.; Weitz, E.; Sachtler, W. M. H. Low Activation Energy Pathway for the Catalyzed Reduction of Nitrogen Oxides to N 2 by Ammonia. *Catal. Lett.* **2004**, *98*, 5−9.
(67) Gordon, I. E.; Rothman, L. S.; Hargreaves, R. J.; Hashemi, R.; Karlovets, E. v.; Skinner, F. M.; Conway, E. K.; Hill, C.; Kochanov, R. v.; Tan, Y.; Wcisło, P.; Finenko, A. A.; Nelson, K.; Bernath, P. F.; Birk, M.; Boudon, V.; Campargue, A.; Chance, K. v.; Coustenis, A.; Drouin, B. J.; Flaud, J. M.; Gamache, R. R.; Hodges, J. T.; Jacquemart, D.; Mlawer, E. J.; Nikitin, A. v.; Perevalov, V. I.; Rotger, M.; Tennyson, J.; Toon, G. C.; Tran, H.; Tyuterev, V. G.; Adkins, E. M.; Baker, A.; Barbe, A.; Canè, E.; Császár, A. G.; Dudaryonok, A.; Egorov, O.; Fleisher, A. J.; Fleurbaey, H.; Foltynowicz, A.; Furtenbacher, T.; Harrison, J. J.; Hartmann, J. M.; Horneman, V. M.; Huang, X.; Karman, T.; Karns, J.; Kassi, S.; Kleiner, I.; Kofman, V.; Kwabia-Tchana, F.; Lavrentieva, N. N.; Lee, T. J.; Long, D. A.; Lukashevskaya, A. A.; Lyulin, O. M.; Makhnev, V. Y.; Matt, W.; Massie, S. T.; Melosso, M.; Mikhailenko, S. N.; Mondelain, D.; Müller, H. S. P.; Naumenko, O. v.; Perrin, A.; Polyansky, O. L.; Raddaoui, E.; Raston, P. L.; Reed, Z. D.; Rey, M.; Richard, C.; Tóbiás, R.; Sadiek, I.; Schwenke, D. W.; Starikova, E.; Sung, K.; Tamassia, F.; Tashkun, S. A.; vander Auwera, J.; Vasilenko, I. A.; Vigasin, A. A.; Villanueva, G. L.; Vispoel, B.; Wagner, G.; Yachmenev, A.; Yurchenko, S. N. The HITRAN2020 Molecular Spectroscopic Database. *J. Quant. Spectrosc. Radiat. Transfer* **2022**, *277*, 107949.

https://doi.org/10.1021/acssuschemeng.3c00208
ACS Sustainable Chem. Eng. 2023, 11, 4289−4298

(68) Bolleter, W. T.; Bushman, C. J.; Tidwell, P. W. Spectrophotometric Determination of Ammonia as Indophenol. *Anal. Chem.* **1961**, *33* (4), 592−594.
(69) Hu, X.; Zhang, Y.; Antonio Wu, R.; Liao, X.; Liu, D.; Cullen, P. J.; Zhou, R.-W.; Ding, T. Diagnostic Analysis of Reactive Species in Plasma-Activated Water (PAW): Current Advances and Outlooks. *J. Phys. D: Appl. Phys.* **2022**, *55*, 023002−023018.
(70) Janda, M.; Hensel, K.; Tóth, P.; Hassan, M. E.; Machala, Z.; Nastuta, V. The Role of HNO 2 in the Generation of Plasma-Activated Water by Air Transient Spark Discharge. *Appl. Sci.* **2021**, *11* (15), 7053−7073.

https://doi.org/10.1021/acssuschemeng.3c00208
ACS Sustainable Chem. Eng. 2023, 11, 4289−4298